

Promising Hard Carbon Coatings on Cu Substrates: Corrosion and Tribological Performance with Theoretical Aspect

A. Madhan Kumar, R. Suresh Babu, I.B. Obot, Akeem Yusuf Adesina, Ahmed Ibrahim, and A.L.F. de Barros

(Submitted September 19, 2017; in revised form November 30, 2017; published online January 19, 2018)

Protecting the surface of metals and alloys against corrosion and wear is of abundant importance owing to their widespread applications. In the present work, we report the improved anticorrosion and tribo-mechanical performance of copper (Cu) by a hard carbon (HC) coating synthesized in different pyrolysis temperature. Structural and surface characterization with roughness measurements was systematically investigated using various techniques. Effect of pyrolysis temperature on the corrosion behavior of coated Cu substrates in 0.6 M NaCl solution was evaluated via electrochemical impedance spectroscopy, potentiodynamic polarization. Pin-on-disk wear test of coated Cu substrate showed the influence of the pyrolysis temperature on the wear resistance performance of the HC coatings. According to the obtained results, it could be concluded that the HC coatings synthesized at 1100 °C revealed an enhanced comprehensive performance, revealing their possible utilization as a protective coating for Cu substrates in chloride environment. Monte Carlo simulations have been utilized to elucidate the interaction between the Cu surface and HC coatings.

Keywords coatings, corrosion, Cu, hard carbon, wear

1. Introduction

Copper (Cu) and its alloys are extensively employed as a structural material in energy conversion, heating and cooling processes, and electronic devices, owing to their excellent mechanical workability, high thermal and electrical conductivity (Ref 1-3). However, the Cu components are extremely vulnerable against corrosion and wear, particularly in marine environments. Through employing diverse coating strategies, it is possible to overcome the corrosion and wear issues of Cu components, and to attain the benefit of a longer service life of coatings for reduction of the total cost.

Owing to high hardness, excellent wear and corrosion resistance, carbon-based materials are often employed as protective

coatings for various metal and alloys against aggressive environments (Ref 4-6). Among the carbon materials, hard carbon (HC) coatings have been matter of extreme consideration due to their fascinating and well suitable properties like chemical inertness, high hardness, low friction coefficient, high wear and electrical resistance, besides good corrosion resistance (Ref 7, 8). HC is a highly disordered or non-graphitizable carbonaceous material; it mainly constructed with two-dimensional ordered graphene sheets can be visualized as house of cards, which are randomly stacked have a turbostratic structure (Ref 9-11). It possesses various defect sites such as cluster gaps, microvoids and atomic dislocations.

Hard carbon coatings are expected to find application to functional thin films for electronic devices and semiconductors, including as constituent film layers in solar cells. Hard carbons have various industrial applications including gas filters, water decolorizes, gas separators, pollution control devices, anode materials for energy storage applications and conversion including Li-ion and Na-ion batteries and supercapacitors (Ref 12, 13).

Herein, we demonstrate the application of synthesized HC samples as protective coatings over Cu substrates in 0.6 M NaCl solution. HC coatings were systematically investigated through structural and surface characterization by x-ray diffraction (XRD) analysis, Raman spectroscopy, scanning electron microscopy (SEM) and optical profilometric techniques. Electrochemical corrosion testing was performed by electrochemical impedance spectroscopic (EIS) and polarization measurements. Further, tribo-mechanical studies have also performed to evaluate their wear characterization with mechanical features.

2. Experimental

2.1 Materials

The HC samples were prepared by pyrolysis method accordance with earlier reports (Ref 14). Briefly, table sugar

Electronic supplementary material The online version of this article (<https://doi.org/10.1007/s11665-018-3148-6>) contains supplementary material, which is available to authorized users.

A. Madhan Kumar and I.B. Obot, Center of Research Excellence in Corrosion, Research Institute, King Fahd University of Petroleum and Minerals, Dhahran 31261, Saudi Arabia; R. Suresh Babu and A.L.F. de Barros, Laboratory of Experimental and Applied Physics, Centro Federal de Educação Tecnológica Celso Suckow da Fonseca, Rio de Janeiro 20271-110, Brazil; Akeem Yusuf Adesina, Mechanical Engineering Department, King Fahd University of Petroleum and Minerals, Dhahran 31261, Saudi Arabia; and Ahmed Ibrahim, Mechanical Engineering Department, King Fahd University of Petroleum and Minerals, Dhahran 31261, Saudi Arabia and Department of Mechanical Design and Production Engineering, Zagazig University, Zagazig 44519, Egypt. Contact e-mails: madhankumar@kfupm.edu.sa and adesina@kfupm.edu.sa.

was dewatered and caramelized at 185 °C for 24 h, then pulverized and kept in tube furnace under argon atmosphere and at temperature about 1100 °C with a ramp of 2 °C min⁻¹. For comparison, the formations of hard carbons were prepared at different temperatures at 600 and 800 °C.

2.2 Preparation of HC Coatings on Cu Substrates

In this present investigation, pure Cu as a base substrate (40 mm × 20 mm × 0.5 mm) was abraded with various grades of emery sheets starting from 320 to 2400. Subsequently, they were cleaned ultrasonically with alcohol to remove the impurities, soaked thoroughly with deionized water and dried by Blast oven. Earlier to all experiment, the Cu substrates were preserved as defined and freshly utilized without storing. Then, synthesized HC samples were applied on Cu substrates through dip-coating technique. Proper amount of the HC samples was dissolved in 1-methyl-2-pyrrolidone (NMP) with constant stirring for 2 h, and the resultant uniform dispersion without settling was utilized. Further, the Cu substrates were then dipped into the HC dispersion and withdrawn from the solution at a constant rate of 100 mm min⁻¹. Consequently, the resultant coated substrates were dried and cured in oven at 100 °C for 24 h. The prepared coatings with the HC synthesized at different temperature from 600 to 1100 °C are abbreviated as HC600, HC800 and HC1100, respectively.

2.3 Structural Characterization

The microstructural characterization of HC was obtained using Raman spectral analysis (Horiba Jobin–Yvon Raman spectrometer, spectrum region of 200–2000 cm⁻¹, laser source of 532 nm, green type). XRD of the synthesized HC was carried out using a RINT2500 with a scattering angle 20° ≤ 2θ ≤ 80° at a 2θ step of 0.02°. X-ray photoelectron spectroscopy (XPS) was performed using ESCALAB-250Xi (Al Kα radiation, 1486.6 eV) to identify the elemental composition of the HC.

2.4 Surface Characterization

The surface microstructure of the coated Cu substrates was observed by SEM analysis (JEOL, JSM-6360). The surface chemical analysis of the coated substrate was made using energy dispersive x-ray spectroscopy (EDS) analysis. Optical profilometer (ContourGT, Bruker, USA) which uses the principle of interferometric was utilized for measuring the microscale roughness of the coatings. 3D images of the samples were obtained by scanning an area of about 1.66 mm × 2.2 mm (3.5 mm²). Three images were captured from different locations on the coated samples with a pixel resolution of 1632 × 786 in order to obtain the arithmetic mean (RA), root-mean-square (RMS) and the peak-to-valley (PV) distance microroughness values.

2.5 Electrochemical Corrosion Tests

Electrochemical corrosion measurement was conducted using a Gamry Instrument potentiostat/galvanostat/ZRA (Reference 3000) with a classical three-electrode cell, placed in a Faraday Cage to diminish noise throughout experiments. A graphite rod and a silver/silver chloride (Ag/AgCl) electrode were served as counter and reference electrodes, respectively.

The Cu substrates with exposed area of 1.766 cm² served as the working electrode. Prior to EIS measurement, the Cu substrate was immersed in the solution for 30 min to acquire a steady open circuit potential (OCP), and then EIS was recorded at OCP in a frequency ranging of 100 kHz–10 mHz with amplitude signal of 10 mV. Further, all electrochemical corrosion data were investigated using Gamry Echem Analyst, version 6.03 software packages. Potentiodynamic polarization tests were carried out through varying the electrode potential range of ± 250 mV from the OCP at a scan rate of 1 mV s⁻¹. All electrochemical corrosion tests were reiterated at least three times to ensure the reproducibility of the obtained results.

2.6 Tribo-Mechanical Characterization

Microindentation test with a pyramidal diamond Vickers indenter was carried out to determine coating micromechanical properties using CSM microindenter (MicroCombi Tester CSM Instruments, Switzerland). Indentation hardness (*H*) and indentation elastic modulus (*E*) were estimated from load–displacement curve according to Oliver and Pharr model (Ref 15). To measure these properties, normal load of 50 mN was applied for 10 s dwell time at loading and unloading rates of 40 mN/min. The applied load was chosen to ensure that the penetration depth does not exceed 10% of the coating thickness.

CSM microindenter (MicroCombi Tester CSM Instruments, Switzerland) was utilized for the scratch test with the standard Rockwell C indenter with 100 μm tip radius. The indenter was pressed against the coating with an initial applied load of 30 mN and then pulled across the coating surface with progressive loading condition until the maximum applied load of 30 N is attained. The scratch test parameters utilized over a scanning length of 10 mm are 5 N/min loading rates and 10 mm/min scratch traverse speed, respectively. During the test, the normal load, penetration depth, acoustic emission (AE), frictional force and the coefficient of friction (COF) were measured. By combining the friction curve and the acoustic emission signal, the critical loads *L_c* were determined and this is the load at which the adhesive failure of the coating occurs (Ref 16).

Wear and friction tests were performed using a multipurpose tribometer (UMT-3, Bruker, USA) with the ball-on-disk configuration. The counterpart is a 6.3-mm diameter stainless steel ball of HRC 62 hardness. The tests were performed in an ambient atmospheric condition at 23 ± 2 °C temperature and 40 ± 5% relative humidity. The experimental parameters for the wear test were as follows: typical wear parameters based on earlier studies (Ref 17, 18) for carbon coatings were utilized; normal load of 10 N was used for a sliding distance of 500 m at 0.14 m/s linear speed, and the wear track diameter is 12 mm. These parameters were selected in order to have sufficient wear to enable distinctive comparison of the HC coated substrates. The wear track cross-sectional area (*A*) of the coating sample was obtained using the optical profilometer (ContourGT, Bruker, USA). Thereafter, the wear volume (*V*) and specific wear rate (*K*) of the coatings were calculated by

$$V = 2\pi rA \quad (\text{Eq 1})$$

$$K = V/SF_N \quad (\text{Eq 2})$$

where *r* refers the radius of the wear track, *S* refers the sliding distance, and *F_N* is the normal applied load.

3. Results and Discussion

3.1 Structural Characterization

Figure 1(a) shows the XRD patterns of the HC600, HC800 and HC1100. Enhanced scattering at low angles of the characteristic features is the presence of two broad bands (002) and (100) diffraction peaks from HC600, HC800 and HC1100 samples, which were broad varying at 2θ of 22.2° - 23.2° and invariant at 43.7° , respectively (Ref 19, 20). This implied that, although either the hybrid amorphous and graphitic nature of carbon had occurred in the HC600, HC800 and increased slowly the degree of graphitization in HC1100. The position of the (002) peak (and thus the d_{002} spacing) has been found to shift to higher angles (i.e., d_{002} spacing decreases) when the pyrolysis temperature increases. The interlayer distance d_{002} for HC600, HC800 and HC1100 is 0.393, 0.386, and 0.381 nm, respectively. There is slight difference in the interlayer distance also for the samples prepared from different pyrolysis temperatures. The result suggests that the formed HC1100 is partially graphitization degree increases during pyrolysis temperature increases. The result suggests that the formed HC1100 is partially (crystalline) graphitization degree increases from amorphous state during pyrolysis temperature from 600 to 1100 °C.

Raman spectroscopy is one of the most extensively used techniques to characterize the structural properties of hard carbon including disorder, defect structures and defect density

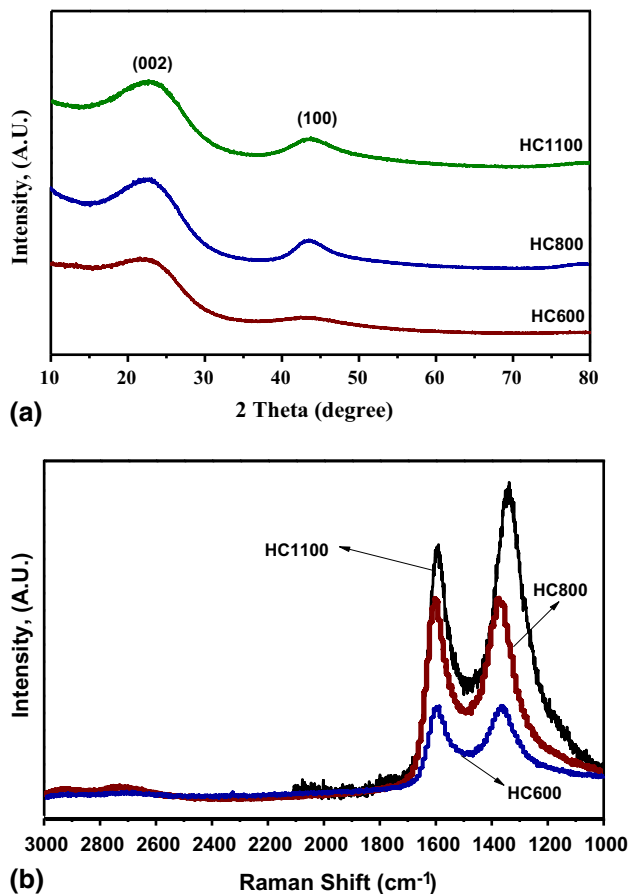


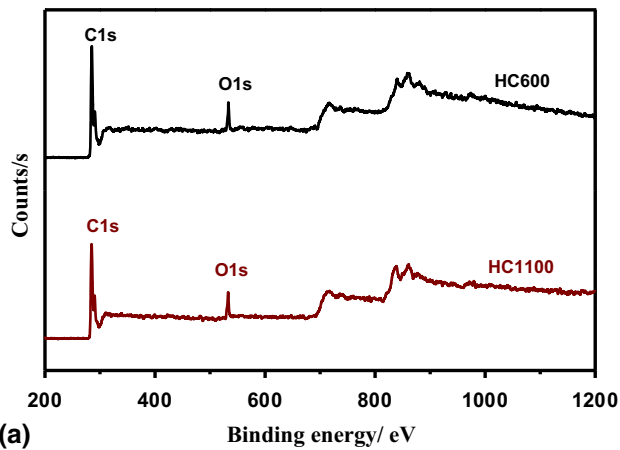
Fig. 1 (a) XRD patterns of HC samples (b) Raman spectra of HC samples

(Ref 21). Figure 1(b) shows the typical Raman spectra of the HC600, HC800 and HC1100 samples. Raman spectra of all the three samples exhibited the two intense bands at the first order region (1100 - 1800 cm^{-1}) corresponding to the disordered carbon (D band) and graphitic carbon (G band), respectively. The D band originated from particle size effects, and G band is related to single crystal graphite. The ratio of the intensities (I_D/I_G) can provide significant information on the structure and domain size of the HC samples. However, the relative intensities of the D to G bands (I_D/I_G), the I_D/I_G values in the spectra of all the three HC samples showed no noticeable change with temperature ranging from 0.99 to 1.02. Although, both the D band and G band peak positions were continuously shifted to higher frequencies, with increases the pyrolysis temperature ranges from 600 to 1100 °C of hard carbon pyrolysis, it reveals sp^2 carbon domain in HC1100 increases, i.e., sp^3/sp^2 ratio increases. In HC600, HC800 and HC1100 the position of G bands was continuously moved from 1460 to 1597 cm^{-1} . The D band on the other hand was gradually shifted from 1281 to 1365 cm^{-1} . High-frequency shift in Raman spectra implied that numerous bond angle disorders were removed and followed by the conversion of sp^3 to sp^2 . In addition, because of thermal annealing, the sp^3 clusters were transformed to sp^2 clusters which results to increase of the sp^2 spots (Ref 22). In HC1100 the structure might be the some amorphous carbon embedding and moderately cross-linking by sp^3 -hybridized carbon atoms and more graphitic (layered) structure fragments consisting of aligned small-dimensionality sp^2 (graphene) layers.

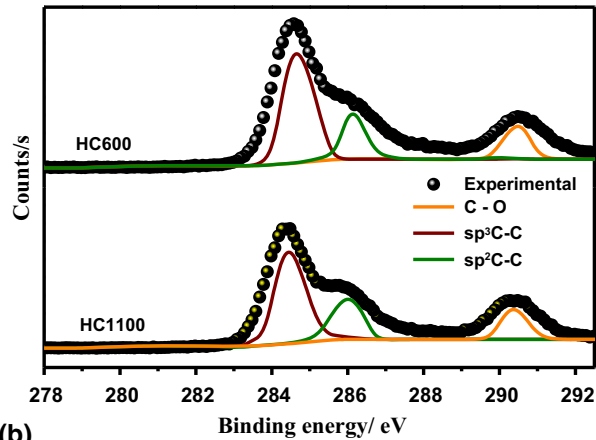
For further analysis, the XPS analysis of HC coatings was performed and the survey spectra are shown in Fig. 2(a). As there was no noticeable variance between HC600 and HC1100, the deconvoluted $C1s$ XPS of HC600 and HC1100 are shown in Fig. 2(b) and (c). As shown in Fig. 2(b) and (c), the $C1s$ peak could be fitted by three components that obtained about 284.8, 286.2, and 290.1 eV, corresponding to sp^3 C-C, sp^2 C-C and C-O, respectively (Ref 22). The supporting information S1 displayed the estimated total volume fraction of bond discretely. As seen in S1, the total fraction of sp^2 C-C increased from 40.24 to 48.32 at.% for HC1100, which revealed that it consists of higher amount of sp^2 -hybridized carbon atoms than HC600. Generally, the hardness and friction coefficient is typically associated with sp^2 fraction (Ref 23). These results are consistent with the Raman analysis the fact that a HC1100 coatings exhibited higher sp^3/sp^2 ratio. Hence, the HC1100 coating might own the highest hardness and lowest friction coefficient among the investigated coatings.

3.2 Surface Characterization

Figure 3 displays representative SEM images of HC coatings synthesized at different pyrolysis temperature. Many pores and defects with emptiness existed at HC600, as seen in Fig. 3(a). In the case of HC800 and HC1100 (Fig. 3b and c), a uniform deposition and relatively smooth surface were obtained. Elemental compositions of the HC coatings were identified by EDS analysis, as presented in Fig. 3(d). It could be implied that the HC coatings were predominantly comprise of C and O elements, which reveals the pure HC coatings on Cu substrate. Further, peak for Fe was not found, corroborating the formation of uniform coatings with no cracks and less porous in nature.



(a)



(b)

Fig. 2 (a) Survey spectra, (b) deconvolution C1s spectra of HC600 and HC1100

The laser microscopy images of HC coating prepared with different synthesized temperature are presented in Fig. 4, and the resultant roughness values of the coatings are shown in Table 1. It is observed that surface roughness properties of the coatings were similar, which indicates that the deposition process is consistent during the coating preparation.

3.3 Electrochemical Corrosion Studies

The typical potentiodynamic polarization curves of coated and uncoated Cu substrates in 0.6 M NaCl solution are shown in Fig. 5. Parameters related to potentiodynamic polarization curves are listed in Table 2. In general, a higher corrosion potential (E_{corr}) or lower corrosion current density (i_{corr}) indicates to a higher corrosion resistance and lower corrosion rate (Ref 24). From the obtained results, it can be observed that the i_{corr} of HC coating is almost two orders of magnitude less than the uncoated Cu substrates. Further, i_{corr} values were decreased with increasing the pyrolysis temperature from 600 to 1100 °C as compared to the uncoated. The significant reduction in the values of i_{corr} of the HC coatings indicates the effective corrosion protection of the Cu substrates. Furthermore, the shift of E_{corr} values toward nobler direction reveals that HC coating mainly confines the anodic dissolution of Cu. It is significant to specify that the HC processed at 1100 °C exhibits more positive potential as compared to the HC processed at other temperatures. The highest protection effi-

ciency is achieved for HC1100 coatings demonstrating its greater corrosion protection performance on Cu substrates.

The illustration of the EIS data as Nyquist plot is displayed in Fig. 6(a). The Nyquist plot of the uncoated Cu substrates comprises of a distorted semicircle at the higher-frequency region followed by a straight line at the lower frequency region. The depressed semicircle is ascribed to the frequency dispersion that caused by the irregularities and heterogeneities of the substrate. The straight line at low-frequency region normally recognized as Warburg impedance (WI) is ascribed to the anodic/cathodic diffusion process at metal/electrolyte interface (Ref 25). And also the existence of WI designates the diffusion reaction rather than charge transfer reaction in this condition. For HC coated Cu substrates, the absence of WI reveals that the electrochemical process at the metal/coating interface could be regulated by the charge transfer reaction as a substitute of the diffusion, contrasting from the uncoated Cu substrates. Further, the diameter of the Nyquist arc in the Cu substrates coated with HC is pointedly larger than that of bare Cu, revealing the polarization resistance has been significantly improved with the presence of HC coating.

EIS bode plots corresponding to the uncoated and coated Cu substrates are shown in Fig. 6(b). The magnitude of the total impedance for the uncoated Cu substrate is measured to be in the range of $10^3 \Omega \text{ cm}^2$ at low-frequency region, signifying that the uncoated Cu substrate readily corrodes; however, in the same frequency region, the $|Z|$ of the coated Cu substrates obstinately increases, specifically for the HC prepared at 1100 °C. In order to deliver comprehensive information about the obtained EIS data, we have proposed the two equivalent circuit models for coated and uncoated Cu substrates in supporting information (S2) and the simulated parameters are listed in Table 3. EIS data of uncoated Cu substrate could be investigated using the equivalent circuit displayed in Fig. S2a, where R_s refers the solution resistance; R_{ct} refers the charge transfer resistance; W is Warburg impedance; and Q_1 refers the constant phase element (CPE) of the double layer capacitance. CPE was substituted in equivalent circuit in order to replace the ideal capacitor to fit the EIS data more accurately. The CPE is mathematically expressed as $Z_{\text{CPE}} = [Y_0 (j \omega)^n]^{-1}$, where Y_0 is CPE constant, n refers the CPE coefficient, and ω refers angular frequency (Ref 26). Constant phase elements Q_2 , and R_f relate to coating layer capacitance and film resistance, respectively.

From Table 3, it could be understood that the double layer capacitance (Q_1) was considerably decreased as a result of the existence of HC coatings which prevent the passage of active species toward Cu surface. From EIS results, it is confirmed that the HC coatings with pyrolysis temperature 1100 °C exhibited highest impedance and lowest double layer capacitance which confirmed the enhanced corrosion protection performance among the investigated coatings. The obtained EIS results further corroborate the interpretations attained from the potentiodynamic polarization studies.

3.4 Tribo-Mechanical Studies

3.4.1 Mechanical Properties. Figure 7(a) displays the measured hardness of HC coatings on Cu substrates. As for the coated Cu substrates, it can be understood that the obtained hardness gradually increases with processing temperature, tending to a maximum value of $\sim 688.77 \text{ MPa}$, which is the intrinsic hardness of the HC coatings. The hardness trend can

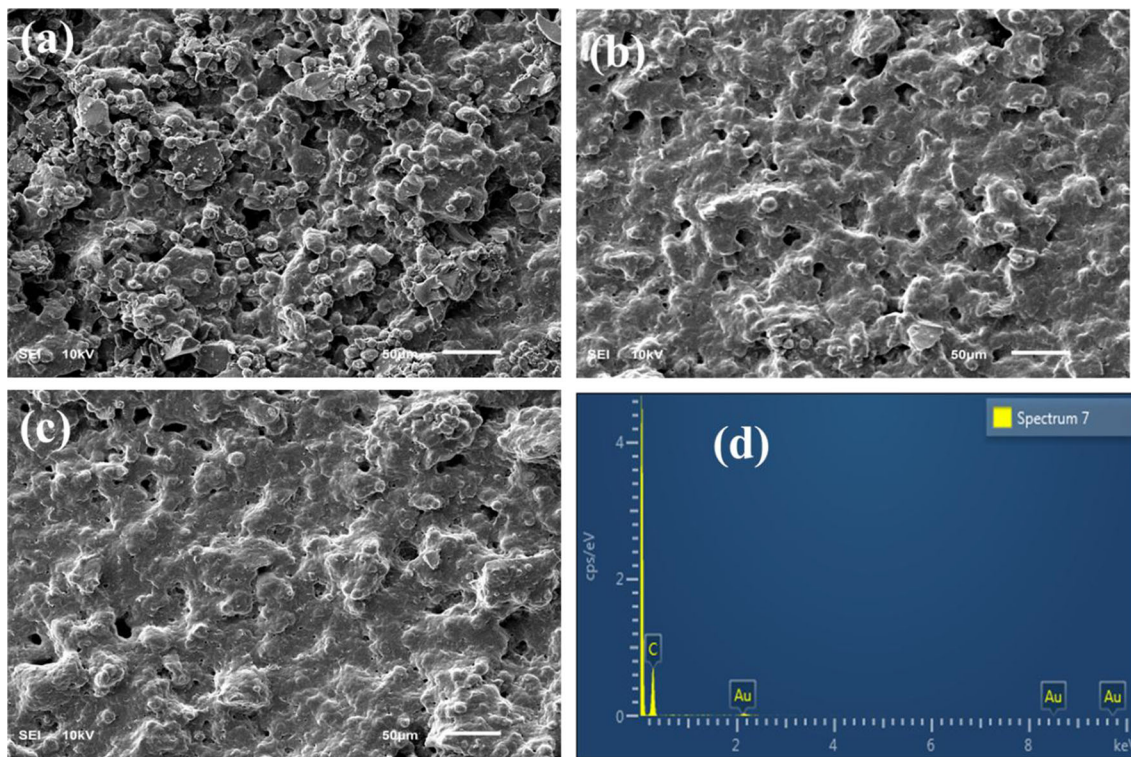


Fig. 3 SEM images of (a) HC600, (b) HC800, (c) HC1100, (d) EDS of HC1100

be associated with increasing carbon content as the processing temperature increases. With higher temperature more sp^2 -hybridized carbon is formed, thus, though the coating deposition parameters are same, the Cu substrates are exposed to different concentration of carbon. The measured hardness of the HC600 and HC800 is 238 and 459.68 MPa, respectively. An increase in the synthesis temperature from 600 to 800 °C causes about 93% increase in the hardness. Furthermore, when the synthesis temperature was increased to 1100 °C as in the HC1100 coating, the hardness increases significantly to about 680 MPa, which is almost 50 and 190% higher than the hardness of HC600 and HC800, respectively, as expected. In addition, results obtained from the microindentation test show that the elastic modulus of the HC600, HC800 and HC1100 coating is 4.51, 6.76, and 9.41 GPa, respectively. This is consistency with typical behavior of the elastic modulus which increases with hardness. The relation between H and E is described through elastic strain to failure and resistance to plastic deformation defined as the ratio H/E and H^3/E^2 , respectively, and it is known that the higher the elastic strain to failure and plastic deformation resistance, the higher is the ratio H/E and H^3/E^2 , respectively (Ref 27, 28). Thus, the elastic strain to failure and plastic deformation resistance of the coating increases in this order HC600 > HC800 > HC1100. To evaluate the adhesive strength of the HC coating toward Cu substrate, the scratch tester was employed in this study. In this test, the adhesive strength is denoted by the critical load (L_c) which is determined by a sudden variation in the acoustic emission signal and the friction force (Ref 29). The higher the critical load the better the coating adhesion to the substrate.

Figure 7(b) shows the critical load of the coating as 12.36, 10.25, and 14.69 N for HC600, HC800 and HC1100, respectively. Based on earlier reports, L_c in the range from 10 to 15 N

is adequate for tribological applications of amorphous carbon coatings and compared to hardness of the coatings this indicates a ductile failure (Ref 29).

3.4.2 Coefficient of Friction and Wear Test. Figure 8(a) displays the friction coefficients of the HC coatings on Cu substrates. It is obvious that the friction curves of HC coated Cu substrates are initiated with a running-in period followed by steady state with almost constant response. It is already described that the coating's defects and high abrasive forces acting at the sliding interface could be strongly influenced the running-in period. When sliding process happened for a while, the contact pressure at the interface is constantly changing alongside the formation of wear debris; however, this did not disturb the progress of the friction coefficient curves, thus long-standing steady-state CoF curve might attained throughout the continued sliding process. Furthermore, it is found that the friction coefficient is similar and they all around 0.2. The CoF of carbon coatings typically below 0.1 steady state (Ref 30-32), however, much higher CoF up to 0.7 has also been reported (Ref 33, 34) based on the composition, the test environments, coating parameters and counterface. In comparison with the other hard coatings (TiN, CrN, etc.), the obtained CoF in this study is low. As reported by other authors (Ref 35, 36), the relatively lower friction coefficient is associated with the formation of a graphite-like lubricious tribo-layer during sliding between the coating and the counterface. This layer could be reason for the low friction due to the availability of hydrogen at the system interface which results in localized annealing of the asperities caused by frictional heating, thus breaking the sp^3 bonds (Ref 34-36).

The specific wear rate was also estimated using Eq 2, it can be observed from Fig. 8(b) that the specific wear rate of HC600, HC800 and HC1100 was 10.30×10^{-4} , 8.73×10^{-4} ,

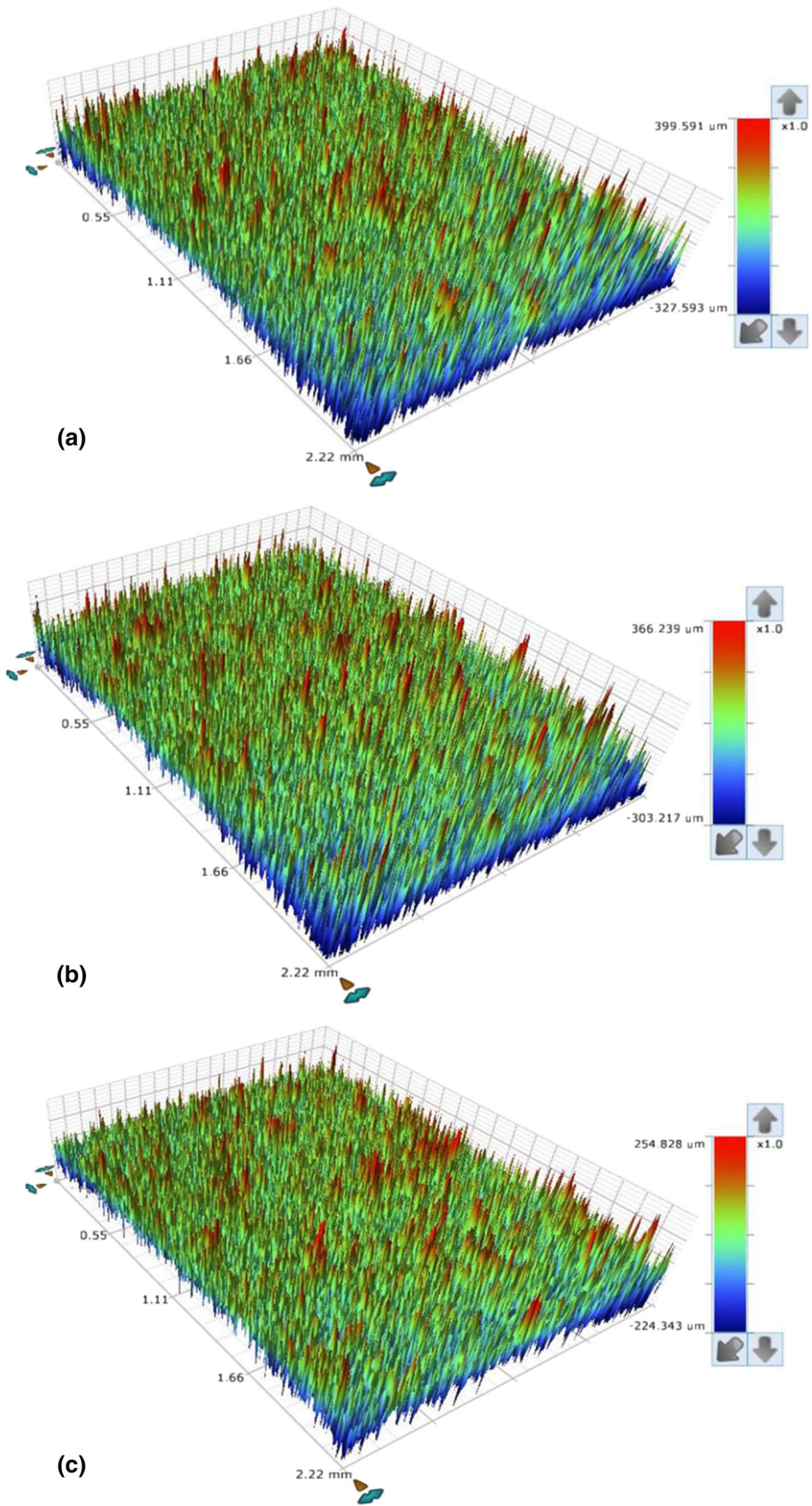


Fig. 4 Surface profile images of (a) HC600, (b) HC800 and (c) HC1100

Table 1 Surface roughness parameters of HC coated Cu substrates

S. no.	Sample	RA, μm	RMS, μm	PV, μm
1	HC600	72.28 ± 3.61	89.32 ± 2.68	599.87 ± 27.60
2	HC800	72.17 ± 2.89	91.47 ± 3.66	669.70 ± 20.09
3	HC1100	75.72 ± 1.51	95.05 ± 3.80	669.46 ± 26.78

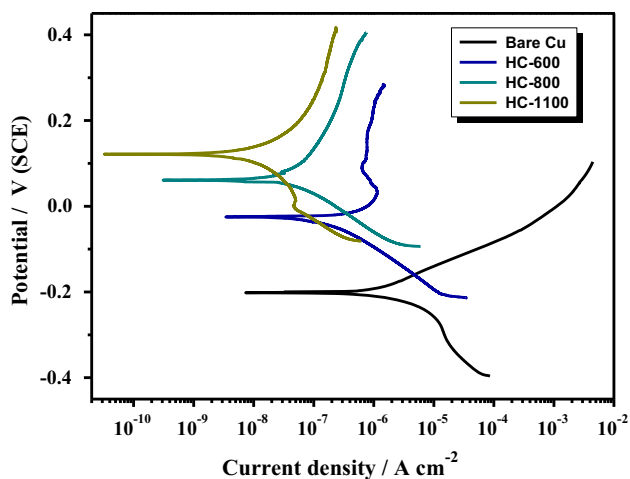


Fig. 5 Potentiodynamic polarization curves of uncoated and coated Cu substrates

Table 2 Tafel parameters of uncoated and HC coated Cu substrates

S. no	Sample	E_{corr} , mV	i_{corr} , $\mu\text{A cm}^{-2}$	Protection efficiency, %
1	Bare Cu	-202	3.710	...
2	HC600	-25.43	0.417	88.76
3	HC800	61.50	0.057	98.46
4	HC1100	121.29	0.015	99.59

and $5.72 \times 10^{-4} \text{ mm}^3/\text{Nm}$, respectively. It is thus observed that the wear rates of HC coated substrates exhibit a decreasing trend with increasing the synthesized temperature of HC, and the least wear rate of $5.72 \times 10^{-4} \text{ mm}^3/\text{Nm}$ for HC1100 coating indicate about 45 and 35% improved wear resistance over HC600 and HC800, respectively. This behavior is obtained owing to the increased quantity of sp^2 -hybridized carbon and enhanced toughness of the coating with temperature. Similar wear rate for hard carbon has also been reported by other authors (Ref 36-38).

Figure 9 shows the typical 3D and 2D profile images of the coatings wear track tested at 10 N normal load and 500 m sliding distance. About three to four depth profile of the wear track from different location along the track was recorded, and the range of depth profile for each of the coating is reported herein. Thus, the profile shows that the wear depth of the HC600 coating is deeper and rougher with more asperities compared to the HC800 and HC1100. The wear track of HC600 coating has a wear depth range of 240-300 μm , HC800 has a wear depth range of 200-280 μm , and the wear depth of HC1100 ranges between 150 and 190 μm only. Also, the wear volume of HC600, HC800 and HC1100 is 5.13, 4.36, and 2.86 mm^3 , respectively. Similar wear resistance behavior has

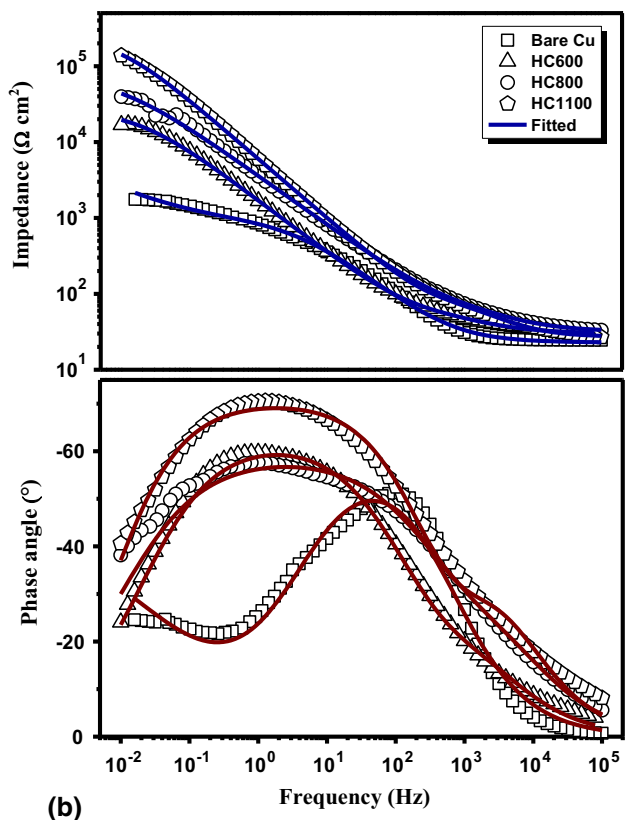
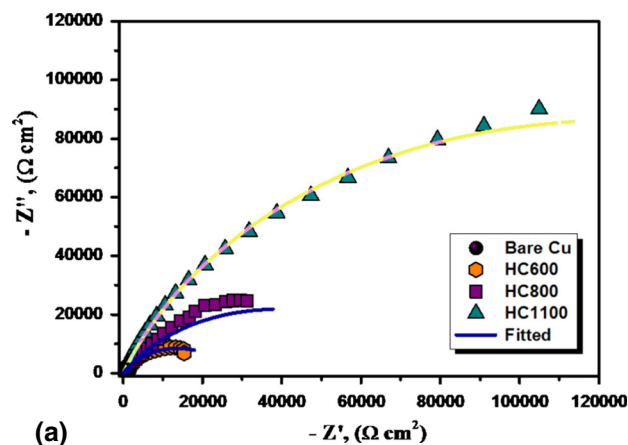


Fig. 6 (a) Nyquist plot, (b) bode plot of uncoated and coated Cu substrates

also been reported for carbon and DLC coating though with different deposition process (Ref 30, 37). The wear volumes of the coatings revealed that HC600 coating has the highest wear volume while HC1100 exhibited the least wear. Therefore, the wear volume increases with decrease in the hardness of the material. This trend follows the Archard's rule of wear volume

Table 3 EIS parameters of uncoated and HC coated Cu substrates

S. no	Sample	$R_s, \Omega \text{ cm}^2$	$Q_1, \mu \text{ F cm}^{-2}$	n_1	$R_f, \text{k}\Omega \text{ cm}^2$	$Q_2, \mu \text{ F cm}^{-2}$	n_2	$R_{ct}, \text{k}\Omega \text{ cm}^2$
1	Bare Cu	22.50		118	0.81
2	HC600	30.10		62.35	0.93	1.75	97.65	0.95
3	HC800	31.25		31.24	0.95	3.49	50.36	0.95
4	HC1100	29.43		17.54	0.96	5.785	23.94	0.97

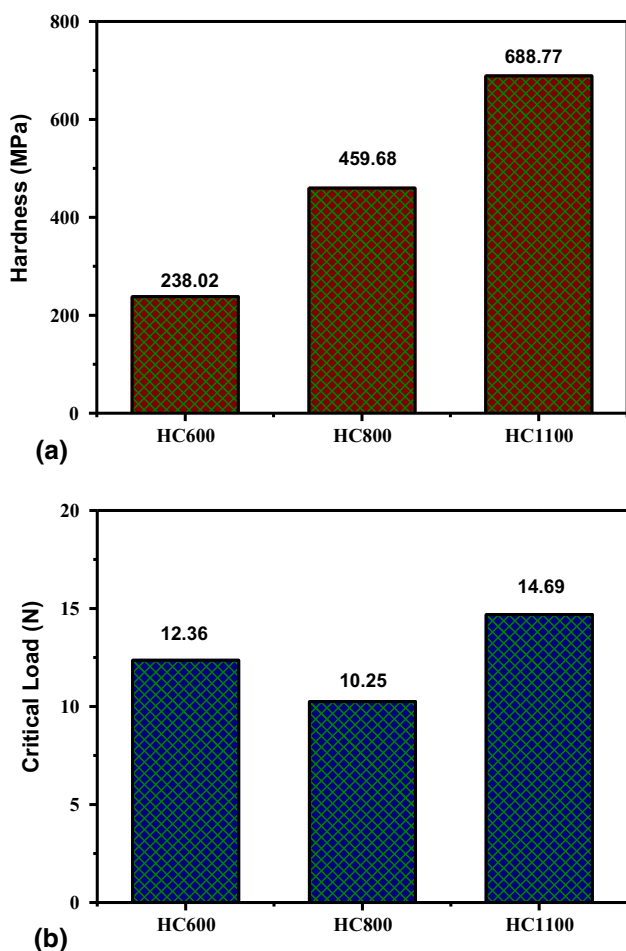


Fig. 7 (a) Hardness and (b) critical load of HC coated Cu substrates

(Ref 39) which postulates that the wear volume loss is inversely proportional to hardness of the soft material which is in this case the coated Cu substrate.

A closer observation of the wear track shows that the wear mechanism is generally adhesive wear due to the presence of removal of chunk of material randomly within the wear track and the absence of fractured wear debris. This behavior is ascribed to the high surface roughness of the coating and the relatively small normal load (10 N) applied. It is also observed that these asperities in contact with the load were mainly plastically deformed rather than fractured. Also new asperities that are gradually been exposed to the normal load may only experience elastic deformation. This explains why the wear

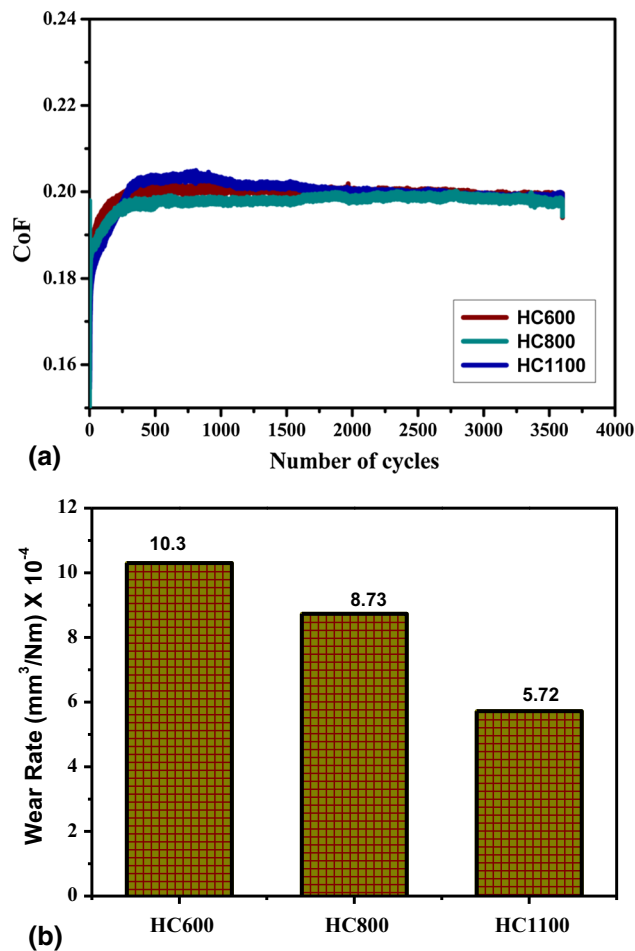


Fig. 8 (a) CoF and (b) wear rate of HC coated Cu substrates

track is not as smooth as expected for a typical wear track. An examination of the stainless steel balls counterface for the three coatings indicate the presence of parallel and narrow scratches on the balls. This concord with the fact that relatively few asperities were in support of the normal load and that these asperities become deformed, while new ones are continuously been exposed during the entire test period (Ref 40).

3.5 Theoretical Simulation Studies

The interaction between the investigated hard carbon coatings and Cu (111) plane surface was carried out using Monte Carlo simulations. The adsorption locator code implemented in the Material Studio 8.0 software from Biovia-Accelrys Inc. USA was adopted in this simulation. The

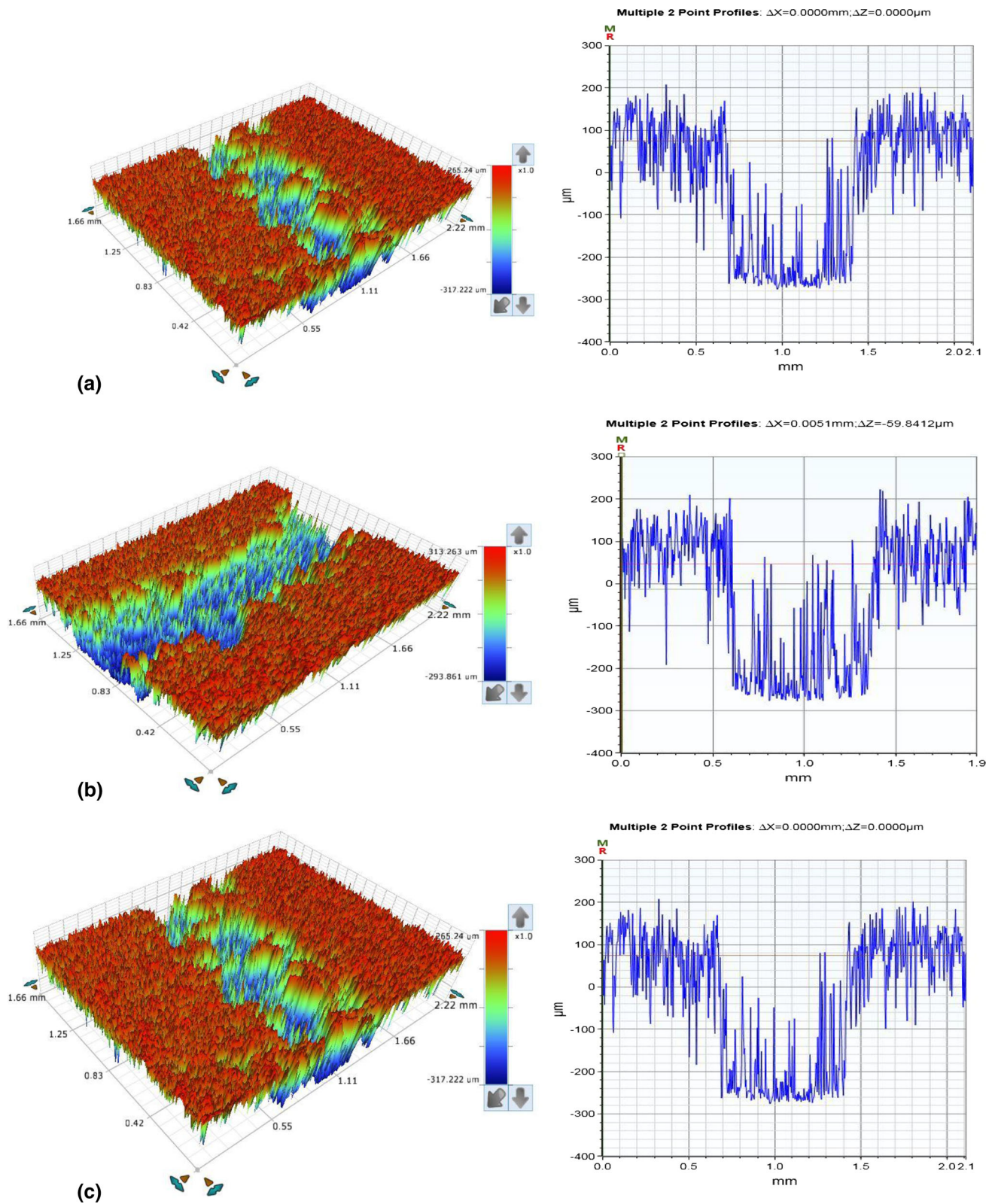
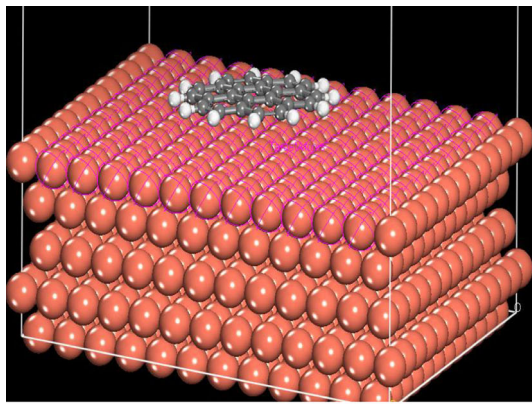


Fig. 9 Surface profile images of (a) HC600, (b) HC800 and (c) HC1100 after wear test

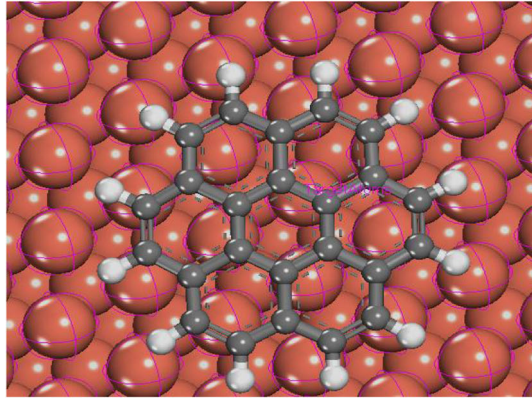
COMPASS (condensed phase optimized molecular potentials for atomistic simulation studies) force field was used for the simulation of all molecules and systems. The simulation of a modeled hard carbon molecule on Cu (111) surface was carried

out in order to locate the low energy adsorption sites and the interaction energy of the hard carbon on Cu surface.

The ability of the model hard carbon molecule to interact with the copper surface is responsible for its improved



(a)



(b)

Fig. 10 (a) Side and (b) top views of the most stable configurations for the adsorption of a hard carbon model on Cu (111) surface calculated using Monte Carlo simulations

Table 4 Outputs and descriptors calculated by Monte Carlo simulation for adsorption of a hard carbon model on Cu (111) surface (in kJ/mol)

Systems	Total energy	Adsorption energy
Cu (111) + graphite	- 181.95	- 407.60

tribological and corrosion protection performance. We simulate the interaction of the hard carbon molecule on the copper electrode surface in order to understand the configuration and the adsorption energies as the hard carbon molecules bond to the copper surface. The top and side views of the most stable adsorption configurations of the model hard carbon on Cu (111) surface using Monte Carlo simulations are shown in Fig. 10(a) and (b). Also, the parameters for the outputs and descriptors acquired from the Monte Carlo simulations are summarized in Table 4. It has been evident from Fig. 10(b) that the modeled hard carbon molecule adsorbed on the copper surface with a parallel orientation in order to increase surface coverage and interaction. It is already been reported that the coating molecules adsorbed almost parallel to the Fe surface delivered the improved corrosion performance. The adsorption at parallel orientation is occurred due to the interaction of the π -electrons of the six membered rings and the lone pair of

electrons of the heteroatoms creating up the coating structures to the iron unfilled d -orbital. These phenomena make a strong chemisorbed bond and hence stable coating on the Fe surface protecting the Fe against corrosion (Ref 41). It is obviously evident from Table 4 that the value of adsorption energy of the modeled hard carbon on Cu (111) surface is high and negative, which signifies that the adsorption could spontaneously occur. The large negative adsorption energy designates the system with the most stable and stronger adsorption (Ref 42, 43). This shows that hard carbon molecule can adsorbed strongly on copper surface thereby preventing copper corrosion. This trend is in agreement with the results obtained experimentally.

4. Conclusions

In this study, the electrochemical and tribo-mechanical properties of hard carbon coatings on Cu substrate were investigated. XRD and Raman spectroscopy confirmed the nature of the crystal structure and graphitization degree of the HC samples synthesized in different pyrolysis temperature. HC1100 coating exhibited hardness of about 680 MPa, which is almost 50 and 190% higher than the hardness of HC600 and HC800, respectively. In addition, results obtained from the microindentation test show that the elastic modulus of the HC600, HC800 and HC1100 coating is 4.51, 6.76, and 9.41 GPa, respectively. Evidence from the wear results specifies that the wear resistance of the HC coated Cu substrates increases with increasing the pyrolysis temperature due to increase in the sp^2 -hybridized carbon and subsequent toughness improvement. At a pyrolysis temperature of 600 °C (HC600), the wear rate was $10.30 \times 10^{-4} \text{ mm}^3/\text{Nm}$, while at 800 °C (HC800) the wear rate reduced to $8.73 \times 10^{-4} \text{ mm}^3/\text{Nm}$. However by increasing the synthesis temperature to 1100 °C (HC1100), the wear rate was reduced beyond 35%. The highest protection efficiency is achieved for HC1100 coatings demonstrating its greater corrosion protection performance on Cu substrates. The large negative adsorption energy obtained by the interaction of the hard carbon with copper surface simulated using Monte Carlo approach shows that hard carbon molecule can be adsorbed strongly on copper surface thereby preventing copper corrosion. According to the obtained results, it could be concluded that HC coatings can be employed as protective coating for Cu substrates in marine environment.

Acknowledgment

The authors gratefully acknowledge King Fahd University of Petroleum and Minerals (KFUPM) for providing the facilities for the research.

Conflict of interest

The authors declare that there is no conflict of interest in the present work.

References

1. M. Finsgar and I. Milosev, Inhibition of Copper Corrosion by 1,2,3-Benzotriazole: A Review, *Corros. Sci.*, 2010, **52**, p 2737–2749

2. N.K. Allam, A.A. Nazeer, and E.A. Ashour, A Review of the Effects of Benzotriazole on the Corrosion of Copper and Copper Alloys in Clean and Polluted Environments, *J. Appl. Electrochem.*, 2009, **39**, p 961–969
3. M.M. Antonijevic and M.B. Petrovic, Copper Corrosion Inhibitors: A Review, *Int. J. Electrochem. Sci.*, 2008, **3**, p 1–28
4. A.Y. Adesina, Z.M. Gasem, and A.M. Kumar, Corrosion Resistance Behavior of Single-Layer Cathodic Arc PVD Nitride-Base Coatings in 1M HCl and 3.5 pct NaCl Solutions, *Metall. Mater. Trans. B*, 2017, **48B**, p 1327–1332
5. A.M. Kumar, M.M. Rahman, and Z.M. Gasem, A Promising Nanocomposite from CNTs and Nanocerria: Nanostructured Fillers in Polyurethane Coatings for Surface Protection, *RSC Adv.*, 2015, **5**, p 63537–63544
6. I.N. Kholmanov, S.H. Domingues, H. Chou, X. Wang, C. Tan, J.Y. Kim, H. Li, R. Piner, A.J.G. Zarkin, and R.S. Ruoff, Reduced Graphene Oxide/Copper Nanowire Hybrid Films as High-Performance Transparent Electrodes, *ACS Nano*, 2013, **7**, p 1811–1816
7. S. Neuville and A. Matthews, A Perspective on the Optimization of Hard Carbon and Related Coatings for Engineering Applications, *Thin Solid Films*, 2007, **515**, p 6619–6653
8. J.S. Chen, Z. Sun, S.P. Lau, and B.K. Tay, Structural and Tribological Properties of Hard Carbon Film Synthesized by Heat-Treatment of a Polymer on Graphite Substrate, *Thin Solid Films*, 2001, **389**, p 161–166
9. H. Hu, G. Chen, and J. Zhang, Synthesis of C60 Nanoparticle Doped Hard Carbon Film by Electrodeposition, *Carbon*, 2008, **46**, p 1091–1109
10. Y. Ohzawa, Y. Yamanaka, K. Naga, and T. Nakajima, Pyrocarbon-Coating on Powdery Hard-Carbon Using Chemical Vapor Infiltration and Its Electrochemical Characteristics, *J. Power Sour.*, 2005, **146**, p 125–128
11. R. Wei, J. Wilbur, A. Erdemir, and F.M. Kustas, The Effects of Beam Energy and Substrate Temperature on the Tribological Properties of Hard-Carbon Films on Aluminum, *Surf. Coat. Technol.*, 1992, **51**, p 139–145
12. W. Xing, R.A. Dunlap, and J.R. Dahn, Studies of Lithium Insertion in Ball Milled Sugar Carbons, *J. Electrochem. Soc.*, 1998, **145**, p 62–70
13. D.A. Stevens and J.R. Dahn, High Capacity Anode Materials for Rechargeable Sodium-Ion Batteries, *J. Electrochem. Soc.*, 2000, **147**, p 1271–1273
14. K. Kuratani, M. Yao, H. Senoh, N. Takeichi, T. Sakai, and T. Kiyobayashi, Na-Ion Capacitor Using Sodium Pre-doped Hard Carbon and Activated Carbon, *Electrochim. Acta*, 2012, **76**, p 320–325
15. W.C. Oliver and G.M. Pharr, Measurement of Hardness and Elastic Modulus by Instrumented Indentation: Advances in Understanding and Refinements to Methodology, *J. Mater. Res.*, 2011, **19**, p 3–20
16. A.J. Perry, Scratch Adhesion Testing of Hard Coatings, *Thin Solid Films*, 1983, **107**, p 167–180
17. H. Ronkainen, J. Likonen, and J. Koskinen, Tribological Properties of Hard Carbon Films Produced by the Pulsed Vacuum Arc Discharge Method, *Surf. Coat. Technol.*, 1992, **54**, p 570–575
18. S. Ghosh, D. Choudhury, T. Roy, A. Bin Mamat, H.H. Masjuki, and B. Pingguan-Murphy, Tribological Investigation of Diamond-Like Carbon Coated Micro-dimpled Surface Under Bovine Serum and Osteoarthritis Oriented Synovial Fluid, *Sci. Technol. Adv. Mater.*, 2015, **16**(3), p 35002
19. Y. Liu, J.S. Xue, T. Zheng, and J.R. Dahn, Mechanism of Lithium Insertion in Hard Carbons Prepared by Pyrolysis of Epoxy Resins, *Carbon*, 1996, **34**, p 193–200
20. A. Gibaud, J.S. Xue, and J.R. Dahn, A Small Angle X-ray Scattering Study of Carbons Made from Pyrolyzed Sugar, *Carbon*, 1996, **34**, p 499–503
21. J. Wang, J.L. Liu, Y.G. Wang, C.X. Wang, and Y.Y. Xia, Pitch Modified Hard Carbons as Negative Materials for Lithium-Ion Batteries, *Electrochim. Acta*, 2012, **74**, p 1–7
22. J. Jin, Z.Q. Shi, and C.Y. Wang, Electrochemical Performance of Electrospun Carbon Nanofibers as Free-Standing and Binder-Free Anodes for Sodium-Ion and Lithium-Ion Batteries, *Electrochim. Acta*, 2014, **141**, p 302–310
23. Y. Ye, Y. Wang, C. Wang, J. Li, and Y. Yao, An Analysis on Tribological Performance of CrCN Coatings with Different Carbon Contents in Seawater, *Tribol. Int.*, 2015, **91**, p 131–139
24. Q.Z. Wang, F. Zhou, X.D. Ding, Z.F. Zhou, C.D. Wang, W.J. Zhang, L.K.Y. Li, and S.T. Lee, Microstructure and Water-Lubricated Friction and Wear Properties of CrN(C) Coatings with Different Carbon Contents, *Appl. Surf. Sci.*, 2013, **268**, p 579–587
25. A.M. Kumar and Z.M. Gasem, Effect of Functionalization of Carbon Nanotubes on Mechanical and Electrochemical Behavior of Polyaniline Nanocomposite Coatings, *Surf. Coat. Technol.*, 2015, **276**, p 416–423
26. G. Gao, B. Yuan, C. Wang, L. Li, and S. Chen, The Anodic Dissolution Processes of Copper in Sodium Fluoride Solution, *Int. J. Electrochem. Sci.*, 2014, **9**, p 2565–2574
27. X. Yufu, Y. Peng, K.D. Dearn, T. You, J. Geng, and H. Xianguo, Fabrication and Tribological Characterization of Laser Textured Boron Cast Iron Surfaces, *Surf. Coat. Technol.*, 2017, **313**, p 391–401
28. Y. Peng, X. Yufu, K.D. Dearn, J. Geng, and H. Xianguo, Novel In Situ Tribo-Catalysis for Improved Tribological Properties of Bio-Oil Model Compound, *Fuel*, 2018, **212**, p 546–553
29. A. Leyland and A. Matthews, On the Significance of the H/E Ratio in Wear Control: A Nanocomposite Coating Approach to Optimized Tribological Behavior, *Wear*, 2000, **246**, p 1–11
30. Y. Peng, X. Yufu, K.D. Dearn, J. Geng, and H. Xianguo, Tribological Assessment of Coated Piston Ring-Cylinder Liner Contacts Under Bio-Oil Lubricated Conditions, *Tribol. Int.*, 2017, **107**, p 283–293
31. Y. Xu, X. Zheng, Y. Yin, J. Huang, and X. Hu, Comparison and Analysis of the Influence of Test Conditions on the Tribological Properties of Emulsified Bio-Oil, *Tribol. Lett.*, 2014, **55**, p 543–552
32. S. Zhang, X.L. Bui, and Y. Fu, Magnetron Sputtered Hard a-C Coatings of Very High Toughness, *Surf. Coat. Technol.*, 2003, **167**, p 137–142
33. D. Camino, A.H.S. Jones, D. Merces, and D.G. Teer, High Performance Sputtered Carbon Coatings for Wear Resistant Applications, *Vacuum*, 1999, **52**, p 125–131
34. Y. Liu, A. Erdemir, and E.I. Meletis, A Study of the Wear Mechanism of Diamond-Like Carbon Films, *Surf. Coat. Technol.*, 1996, **82**, p 48–56
35. A. Grill and V. Patel, Tribological Properties of Diamond-Like Carbon and Related Materials, *Diam. Relat. Mater.*, 1993, **2**, p 597–605
36. K.C. Walter, H. Kung, T. Levine, J.T. Tesmer, P. Kodali, B.P. Wood, D.J. Rej, M. Nastasi, J. Koskinen, and J.P. Hirvonen, Characterization and Performance of diamond-Like Carbon Films Synthesized by Plasma- and Ion-Beam-Based Techniques, *Surf. Coat. Technol.*, 1995, **74**, p 734–738
37. Y. Liu, A. Erdemir, and E.I. Meletis, An Investigation of the Relationship Between Graphitization and Frictional Behavior of DLC Coatings, *Surf. Coat. Technol.*, 1996, **86**, p 564–568
38. S. Yang, D. Camino, A.H. Jones, and D. Teer, Deposition and Tribological Behavior of Sputtered Carbon Hard Coatings, *Surf. Coat. Technol.*, 2000, **124**, p 110–116
39. S.K. Field, M. Jarratt, and D.G. Teer, Tribological Properties of Graphite-Like and Diamond-Like Carbon Coatings, *Tribol. Int.*, 2004, **37**, p 949–956
40. A.M. Kumar, E. Thangavel, S. Ramakrishna, I.B. Obot, H.C. Jung, K.S. Shin, Z.M. Gasem, H. Kim, and D.-E. Kim, Multi-functional Ceramic Hybrid Coatings on Biodegradable AZ31 Mg Implants: Electrochemical, Tribological and Quantum Chemical Aspects for Orthopaedic Applications, *RSC Adv.*, 2014, **4**, p 24272–24285
41. A.M. Kumar, R.S. Babu, I.B. Obot, and Z.M. Gasem, A Promising Nanocomposite from CNTs and Nanocerria: Nanostructured Fillers in Polyurethane Coatings for Surface Protection, *RSC Adv.*, 2015, **5**, p 19264–19272
42. I.B. Obot, I.B. Onyeachu, and A.M. Kumar, Sodium Alginate: A Promising Biopolymer for Corrosion Protection of API, X60 High Strength Carbon Steel in Saline Medium, *Carbohydr. Polym.*, 2017, **178**, p 200–208
43. A.M. Kumar, B. Suresh, S. Ramakrishna, and K.S. Kim, Biocompatible Responsive Polypyrrole/GO Nanocomposite Coatings for Biomedical Applications, *RSC Adv.*, 2015, **5**, p 99866–99874